High-order numerical methods for LES of turbulent flows with shocks

By D. Kotov, H.C. Yee†, A. Hadjadj‡, A. Wray† AND B. Sjögreen¶

1. Motivation and objectives

The presence of a shock wave in the flow field might pose a particular problem in employing the LES filtered equations across discontinuities, depending on the LES model, the grid size, and shock strength. Since the majority of dynamic LES models involve filter operations, hereafter referred to as LES filters, to distinguish them from standard numerical filters, when the LES filtered equations are applied through the shock, the Rankine-Hugoniot relations are affected by the filtering operation as the filtered variable is not discontinuous. Sagaut & Germano (2005) have noticed that the usual filtering procedures, based on a central spatial filter that provides information from both sides, when applied around the discontinuity, produce parasitic contributions that affect the filtered quantities. They suggested using non-centered filters to avoid this nonphysical effect. In Grube & Martin (2009) shock-confining filters have been proposed instead of using centered filters. A completely different approach based on deconvolution method is considered in Adams & Stolz (2002).

The accuracy of filtering procedure depends on the precision of the numerical identification of the shock wave location. In this study we consider a combination of the low-dissipative high-order nonlinear filter scheme of Yee & Sjögreen (2007) to locate the discontinuity accurately, and the subcell resolution method of Harten (1989) to confine the discontinuity location to be within a grid cell. Previous studies indicate that the combination of the nonlinear filter scheme with Harten's subcell resolution method is able to locate the discontinuity within a grid cell very accurately. A new accurate method to handle the transition points (buffer zone) between the smeared shock wave and the one-sided LES filter equations is under development. Here we will also consider the modification of LES filtering procedure including local one-sided filtering without subcell resolution. Another modification considered here is local disabling of subgrid-scale (SGS) dissipation, which has been employed in some previous studies, e.g., Hadjadj & Dubos (2009); Bermejo-Moreno *et al.* (2010).

In the present study we consider LES with implicit filtering employing the dynamic Germano procedure (Germano *et al.* 1991) for calculating model coefficients. Therefore, all aforementioned modifications of LES filtering procedure refer to the Germano model and do not affect the LES in other ways. However, in the case of LES with explicit filtering, similar procedures should be applied to explicit LES filtering as well.

† NASA Ames Research Center
‡ CORIA UMR 6614 & INSA de Rouen, France
¶ Lawrence Livermore National Laboratory

2. Mathematical formulation and numerical methods

2.1. *Governing equations & LES model*

We consider the governing equations written as

$$\partial_t \bar{\rho} + \partial_j(\bar{\rho}\tilde{u_j}) = 0, \tag{2.1}$$

$$\partial_t(\bar{\rho}\tilde{u_i}) + \partial_j(\bar{\rho}\tilde{u_i}\tilde{u_j} + \bar{p}\delta_{ij} - \check{\tau}_{ij} + \tau^S_{ij}) = 0, \tag{2.2}$$

$$\partial_t(\bar{\rho}\tilde{E}) + \partial_j(\bar{\rho}\tilde{E}\tilde{u_j} + \bar{p}\tilde{u}_j - \check{\tau}_{ij}\tilde{u}_i + \check{q}_j + q^S_j) = 0, \tag{2.3}$$

where ρ is the density, u_i is the i^{th} velocity component, p is the pressure, T is the temperature, E is the total energy, and t is the time. For the given f, a LES filtering operation is denoted as $\bar{f}$. The Favre filtering operation is denoted as $\tilde{f} = \overline{\rho f}/\bar{\rho}$, and $\check{f}$ stands for the function of Favre-filtered variables, defined as

$$\check{\tau}_{ij} = 2\mu(\tilde{T})(\tilde{S}_{ij} - \frac{1}{3}\delta_{ij}\partial_k\tilde{u}_k), \quad \tilde{S}_{ij} = (\partial_j\tilde{u}_i + \partial_i\tilde{u}_j)/2, \quad \check{q}_j = -\lambda(\tilde{T})\partial_j\tilde{T}, \tag{2.4}$$

where dynamic viscosity is given by $\mu(T) = \mu_0(T/T_0)^{3/4}$, thermal conductivity is expressed through a constant Prandtl number Pr, and heat capacity at constant pressure c_p: $\lambda(T) = c_p\mu(T)/\mathrm{Pr}$. The equation of state is $\bar{p} = R\bar{\rho}\tilde{T}$, where R is a gas specific constant. The subgrid-scale (SGS) terms, SGS stress tensor τ^S_{ij}, and SGS heat flux q^S_j are modeled as

$$\tau^S_{ij} - \frac{1}{3}\tau^S_{kk}\delta_{ij} = -2\mu_t(\tilde{S}_{ij} - \frac{1}{3}\tilde{S}_{kk}\delta_{ij}), \quad \tau^S_{kk} = 2C_I\bar{\rho}\Delta^2|\tilde{S}|^2, \quad q^S_j = \frac{\mu_t\gamma c_v}{\mathrm{Pr}_t}\partial_j\tilde{T}, \tag{2.5}$$

where $\mu_t = \bar{\rho}C_s\Delta^2|\tilde{S}|$, $|\tilde{S}| = \sqrt{2\tilde{S}_{ij}\tilde{S}_{ij}}$, and Δ is filter width. The Smagorinsky constant C_s and the constant for isotropic part of the SGS stress C_I are obtained through the Germano-Lilly (Germano *et al.* (1991); Lilly (1992)) procedure, which can be written as

$$C_s = \frac{\left\langle L^{C_s}_{ij} M^{C_s}_{ij} \right\rangle_H}{\left\langle M^{C_s}_{ij} M^{C_s}_{ij} \right\rangle_H}, \qquad C_I = \frac{\langle L_{ll} \rangle_H}{\left\langle M^{C_I}_{ll} \right\rangle_H}, \tag{2.6}$$

where

$$L^{C_s}_{ij} = L_{ij} - \frac{1}{3}L_{ll}\delta_{ij}, \qquad L_{ij} = \left(\widehat{\bar{\rho}\tilde{u}_i\tilde{u}_i}\right) - \widehat{\bar{\rho}\tilde{u}_i}\widehat{\bar{\rho}\tilde{u}_i}/\hat{\bar{\rho}}, \tag{2.7}$$

$$M^{C_s}_{ij} = -2\hat{\bar{\rho}}\hat{\Delta}^2|\hat{\tilde{S}}|^2\left(\tilde{S}_{ij} - \widehat{\frac{1}{3}\tilde{S}_{ll}\delta_{ij}}\right) + 2\Delta^2\left[\left(\widehat{\bar{\rho}|\tilde{S}|\tilde{S}_{ij}}\right) - \frac{1}{3}\left(\widehat{\bar{\rho}|\tilde{S}|\tilde{S}_{ll}}\delta_{ij}\right)\right], \tag{2.8}$$

$$M^{C_I}_{ll} = 2\hat{\bar{\rho}}\hat{\Delta}^2|\hat{\tilde{S}}|^2 - 2\Delta^2\left(\widehat{\bar{\rho}|\tilde{S}|^2}\right), \tag{2.9}$$

and $< f >_H$ stands for averaging in homogeneous directions.

For the considered test case with low turbulent Mach number $\mathrm{M}_t < 0.4$, Erlebacher *et al.* (1992) showed that the isotropic part of SGS stress can be neglected: $C_I = 0$. The Germano procedure requires an explicit filtering operation, denoted here with the bar symbol. For the Germano procedure, we use a 3D filtering operator based on a 1D trapezoidal filter, discretized as

$$\hat{f}_i = \frac{1}{4}f_{i-1} + \frac{1}{2}f_i + \frac{1}{4}f_{i+1}. \tag{2.10}$$

Note that according to Lund (1997), the width of the discrete filter can be estimated

as

$$\Delta = h\sqrt{12\sum_{j=-(N-1)/2}^{(N-1)/2} j^2 W_j}, \tag{2.11}$$

where h is the grid spacing and W_j are the filter weights. Using Eq. (2.11) for the filter Eq. (2.10) gives $\Delta = h\sqrt{6}$.

2.2. *High-order filter schemes*

In order to solve the system (2.1) – (2.3) by introducing as little numerical dissipation as possible, we use the high-order nonlinear filter scheme of Yee & Sjögreen (2007), which consists of three steps.

2.2.1. *Pre-processing step*

Before the application of a high-order non-dissipative spatial base scheme, a preprocessing step is employed to improve the stability. The inviscid flux derivatives of the governing equations are split in the following three ways, depending on the flow types and the desire for rigorous mathematical analysis or physical argument.

1. Entropy splitting of Olsson & Oliger (1994) and Yee *et al.* (2000); Yee & Sjögreen (2002). The resulting form is non-conservative and the derivation is based on entropy norm stability with boundary closure for the initial value boundary problem.

2. The system form of the Ducros *et al.* (2000) splitting. This is a conservative splitting formulation, and the derivation is based on physical arguments.

3. Tadmor entropy conservation formulation for systems Sjögreen & Yee (2009). The derivation is based on mathematical analysis. It is a generalization of Tadmor's entropy formulation to systems and has not been fully tested on complex flows.

2.2.2. *Base scheme step*

A full time step is advanced using a high-order non-dissipative (or very low dissipation) spatially central scheme on the split form of the governing partial differential equations (PDEs). A summation-by-parts (SBP) boundary operator (Olsson 1995; Sjögreen & Yee 2007) and matching order conservative high-order free stream metric evaluation for curvilinear grids (Sjögreen *et al.* 2014) are used. High-order temporal discretization such as the third-order or fourth-order Runge-Kutta (RK3 or RK4) method is used. Other temporal discretizations can be used for the base scheme step.

2.2.3. *Post-processing (nonlinear filter step)*

To further improve nonlinear stability from the non-dissipative spatial base scheme, after the application of a non-dissipative high-order spatial base scheme in the split form of the governing equation(s), the post-processing step is used to nonlinearly filter the solution by a dissipative portion of a high-order shock-capturing scheme with a local flow sensor. The flow sensor provides locations and amounts of built-in shock-capturing dissipation that can be further reduced or eliminated. At each grid point, a local flow sensor would be employed to analyze the regularity of the computed flow data. Only the discontinuity locations would receive the full amount of shock-capturing dissipation. In smooth regions, no shock-capturing dissipation would be added. In regions with strong turbulence, a small fraction of the shock-capturing dissipation would be added to improve stability. For the problem considered in this work, we use the flow sensor of Ducros *et al.*

(1999) which can be written as

$$w = \frac{(\nabla \cdot \mathbf{u})^2}{(\nabla \cdot \mathbf{u})^2 + \omega^2 + \varepsilon}. \tag{2.12}$$

Here $\mathbf{u}$ is the velocity vector, ω is the vorticity magnitude, and $\varepsilon = 10^{-6}$ is a small number to avoid division by zero. The nonlinear dissipative portion of a high-resolution shock-capturing scheme can be any shock-capturing scheme. For the problem considered in this study, it is activated when the Ducros et al. sensor $w > 0.6$ for the case M = 1.5 and $w > 0.3$ for the case M = 3.

Let U^* be the solution after the completion of the base scheme step. The final update of the solution after the filter step is (with the numerical fluxes in the y- and z-directions suppressed, as well as their corresponding y- and z-direction indices on the x inviscid flux suppressed)

$$U^{n+1}_{j,k,l} = U^*_{j,k,l} - \frac{\Delta t}{\Delta x}[H^*_{j+1/2} - H^*_{j-1/2}], \quad H_{j+1/2} = R_{j+1/2}\overline{H}_{j+1/2}, \tag{2.13}$$

where $R_{j+1/2}$ is the matrix of right eigenvectors of the Jacobian of the inviscid flux vector in terms of Roe's average states based on U^*. $H^*_{j+1/2}$ and $H^*_{j-1/2}$ are numerical fluxes in terms of Roe's average states based on U^*. Denote the elements of the vector $\overline{H}_{j+1/2}$ by $\overline{h}^l_{j+1/2}, l = 1, 2, ..., 5$. The nonlinear portion of the filter $\overline{h}^l_{j+1/2}$ has the form

$$\overline{h}^l_{j+1/2} = \frac{\kappa}{2} w^l_{j+1/2} \phi^l_{j+1/2}. \tag{2.14}$$

Here $w^l_{j+1/2}$ is the flow sensor to activate the nonlinear numerical dissipation $\frac{1}{2}\phi^l_{j+1/2}$, and the original formulation for κ is a positive parameter that is less than or equal to 1. The choice of the parameter κ can be different for different flow types. However, in this study we set $\kappa = 1$.

Note that the nonlinear filter step described above should not be confused with the LES filtering operation.

2.3. *Modifications of the LES filtering procedure for flows with shocks*

During a LES computation using the formulation above, there are two additional sources of inaccuracy that appear in the vicinity of the shock. The first one is connected with the numerical scheme used for solving the governing equation. Away from the shock, the high-order central scheme is applied, introducing negligible amount of numerical dissipation. However, in the vicinity if the shock, the shock-capturing scheme is activated, causing a significant amount of dissipation to be introduced into the results. The amount of numerical dissipation introduced by the shock-capturing scheme, depending on the particular problem parameters, may be higher than the turbulent dissipation modeled by SGS terms. In this case, it might be reasonable to locally disable the SGS terms in order to obtain more accurate results (Hadjadj & Dubos 2009; Bermejo-Moreno *et al.* 2010). LES with this filtering procedure is denoted as LES-Z.

The second additional source of inaccuracy of LES results in the vicinity of the shock derives from the fact that the explicit filtering operation in Eqs. (2.6 – 2.9) is applied across the discontinuity, causing too much smearing of the results. In this case, as Sagaut & Germano (2005) pointed out, a one-sided filtering operation should be used instead of the central one for all points near the shock. LES with this filtering procedure is denoted as LES-1S.

3. Turbulence across a supersonic shock wave

3.1. *Problem setup*

The problem considered here has been studied extensively, e.g., Lee *et al.* (1997); Larsson & Lele (2009); Bermejo-Moreno *et al.* (2010). Here we have chosen the configuration considered in Larsson & Lele (2009). The computational domain is 4π in X (streamwise) and $2\pi \times 2\pi$ in Y and Z (transverse) directions. The grid is uniform in all directions, with the spacing in X three times finer than that in Y and Z (see Larsson & Lele (2009) for explanation). In order to obtain more accurate results, we use WENO dissipation only in the X direction at the postprocessing stage of the Yee et al.'s filter scheme. The inflow and outflow boundary conditions are applied in the streamwise direction, and periodic boundary conditions are applied in the transverse directions. The initial conditions include shock in the $X = 0$ plane.

Inflow boundary condition: A fully developed turbulent inflow condition is applied using inflow turbulent database. This database is generated as follows. First, an initial isotropic turbulent field with the energy spectra $E(k) \sim k^4 \exp(-2k^2/k_0^2)$ and microscale Reynolds number $\mathrm{Re}_\lambda = \rho\lambda u'_{rms}/\mu = 140$ is generated using the methodology of Ristorcelli & Blaisdell (1997). Here, an energy peak wavenumber $k_0 = 4$ is used. Next, the decay of this field in periodic box is simulated for approximately three eddy turnover times $\tau = \lambda/u'_{rms}$ to ensure that turbulence is fully developed. After the decay, the Reynolds number $\mathrm{Re}_\lambda = 40$ and the turbulent Mach number is $\mathrm{M}_t = \overline{u'_i u'_i}^{1/2}/c_0 = 0.16$. The field obtained in this isotropic turbulence simulation is introduced at the inflow boundary with constant mean velocity u_0. We consider two cases, with mean flow Mach number $\mathrm{M} = 1.5$ and $\mathrm{M} = 3.0$.

Outflow boundary condition: In order to avoid acoustic reflections of subsonic flow from the outflow boundary, a sponge is employed on the region near the outflow. The length of the region is $x_{max} - x_{sp} = \pi$. The sponge is implemented by introducing the source term to the Eqs. (2.1 – 2.3), given by the form

$$\Omega = -\frac{k_0 u_0}{2\pi}\left(\frac{x - x_{sp}}{x_{max} - x_{sp}}\right)(f - < f >_{yz}), \tag{3.1}$$

where $f = \rho, \rho u_i, E$ and $\langle\cdot\rangle_{yz}$ denotes averaging in Y and Z directions. The outflow pressure p_∞ is chosen such that the mean shock location is stationary. See (Larsson & Lele 2009) for more details.

Gathering statistics: The simulation statistics is obtained by averaging in time and in homogeneous directions. The averaging is performed over time range $\Delta t \approx 100/(k_0 u_0)$. The convergence is confirmed by comparing the results with the statistics obtained over time range $\Delta t/2$. The statistics is gathered after the transition period has passed. Transient time t_0 is estimated as $t_0 \gg L_x/u_0$, where L_x is the domain size in the streamwise direction. The correct choice of transient time is confirmed by comparing with the statistics obtained starting from time $t_0/2$.

3.2. *DNS results*

The DNS results are obtained on a grid of 1553×256^2 points. The instantaneous streamwise and transverse velocity contours are shown in Figure 1. During the simulation over long period of time, the shock moved slightly upstream. The shock is wrinkled due to turbulent inflow. As shown in previous studies (Lee *et al.* 1997; Larsson & Lele 2009), the shock may break at higher turbulent Mach numbers M_t. The turbulence is compressed by the shock, and immediately behind the shock, it is anisotropic. The turbulence becomes

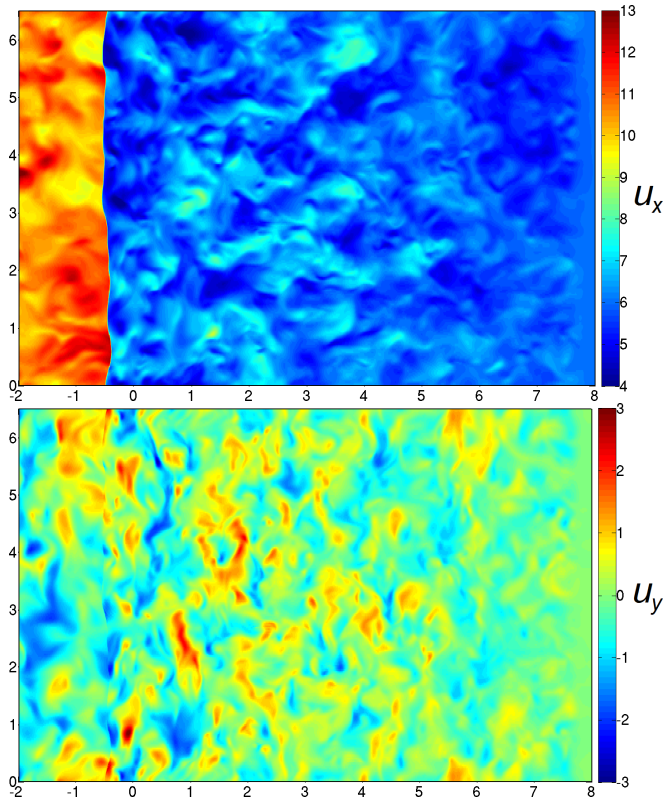

FIGURE 1. Instantaneous velocity u_x (top) and u_y (bottom) contour obtained in DNS on grid 1553×256^2. Slice $z = \text{const}$.

isotropic again downstream of $x \approx 3$. Downstream of $x = 8$, the turbulence is essentially dumped with the sponge source term.

The comparison of the DNS statistics obtained in this work using ADPDIS3D code with the data obtained from digitizing the solution from Larsson & Lele (2009) is shown in Figure 2. The results are in good agreement. The grid resolution in the vicinity of the shock is the same. In Larsson & Lele (2009), grid clustering near the shock has been employed, resulting in a smaller grid size of 694×256^2 points. Larsson & Lele (2009) employed HYBRID code, which also uses the Ducros et al. flow sensor for shock detection. However, in Larsson & Lele (2009), the WENO dissipation has been introduced at every Runge-Kutta stage, whereas the Yee et al. scheme allows the computational cost to be decreased by introducing WENO dissipation only after the full-time Runge-Kutta step. In this study, we use a uniform grid to allow for straightforward comparison of the schemes.

3.3. *LES results*

In this section we compare the results obtained by Germano LES using different filtering procedures (LES with standard filtering procedure, LES-Z and LES-1S) with DNS solution filtered to the size of the LES grid. We do not show results obtained by LES-SR, since this method is still under development.

Comparison of the methods on a 389×64^2 grid for the case M = 1.5 is shown in Figures 3, 4. For this case, the results obtained using LES-Z, and LES-1S are closer to filtered DNS than to standard LES. LES-1S performs a little better then LES-Z. The

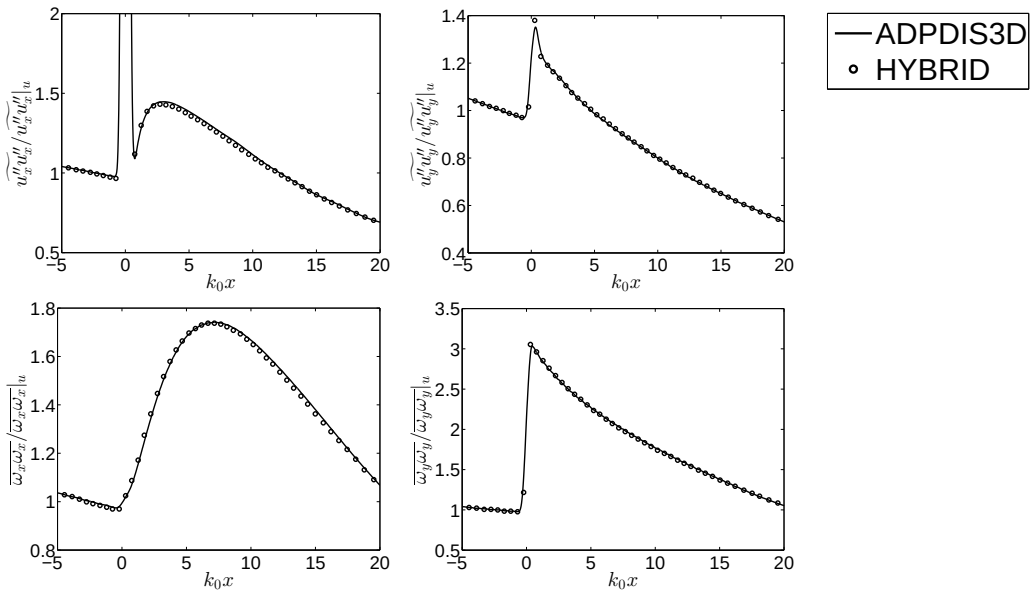

FIGURE 2. Comparison of DNS statistics obtained in this work employing ADPDIS3D code with the data obtained from digitizing the solution Larsson & Lele (2009) employing HYBRID code. Top row: Reynolds Stress components X (left) and Y (right). Bottom row: vorticity components X (left) and Y (right).

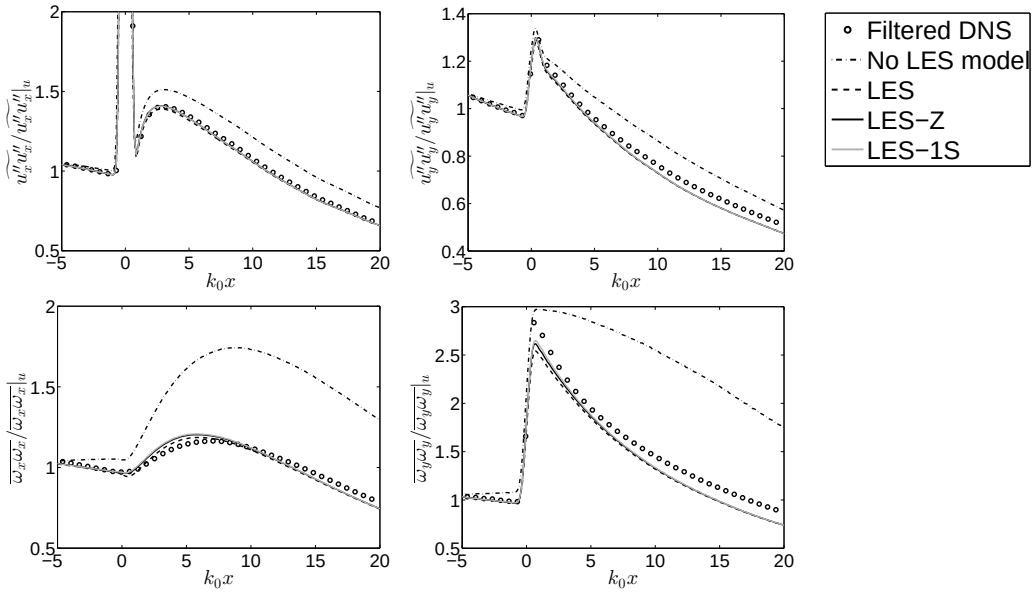

FIGURE 3. Comparison of filtered DNS data with the statistics obtained by LES with different filtering procedures (standard LES, LES-Z and LES-1S) on coarse grid 389×64^2, M = 1.5. Top row: Reynolds Stress components X (left) and Y (right). Bottom row: vorticity components X (left) and Y (right).

behavior of the methods is similar in the M = 3 case (see Figure 5), but LES-Z in this case performs slightly better than LES-1S. Also, similar behavior has been obtained on

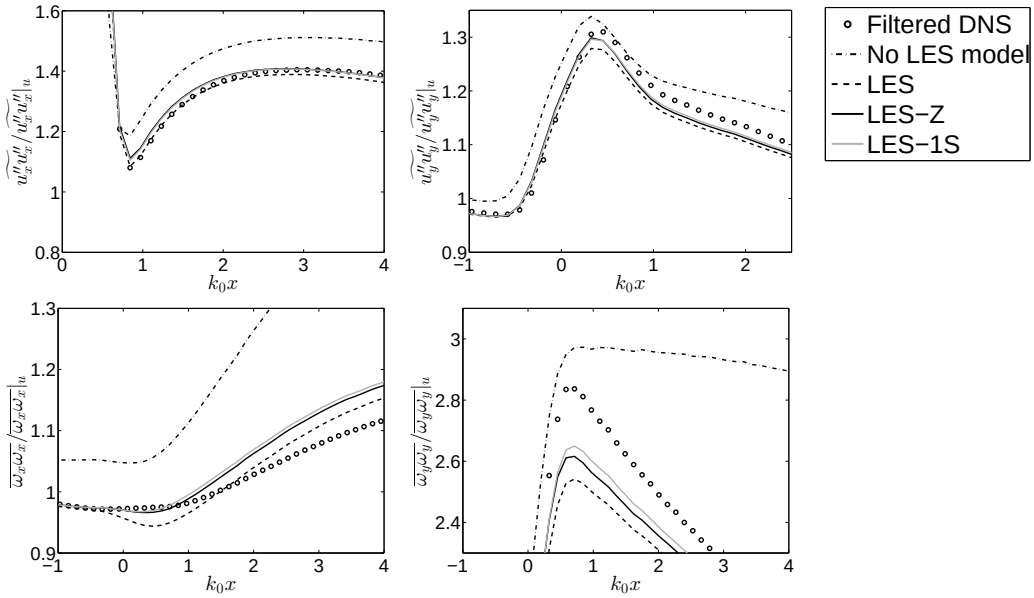

FIGURE 4. Same as Figure 3, zoom in the vicinity of the shock

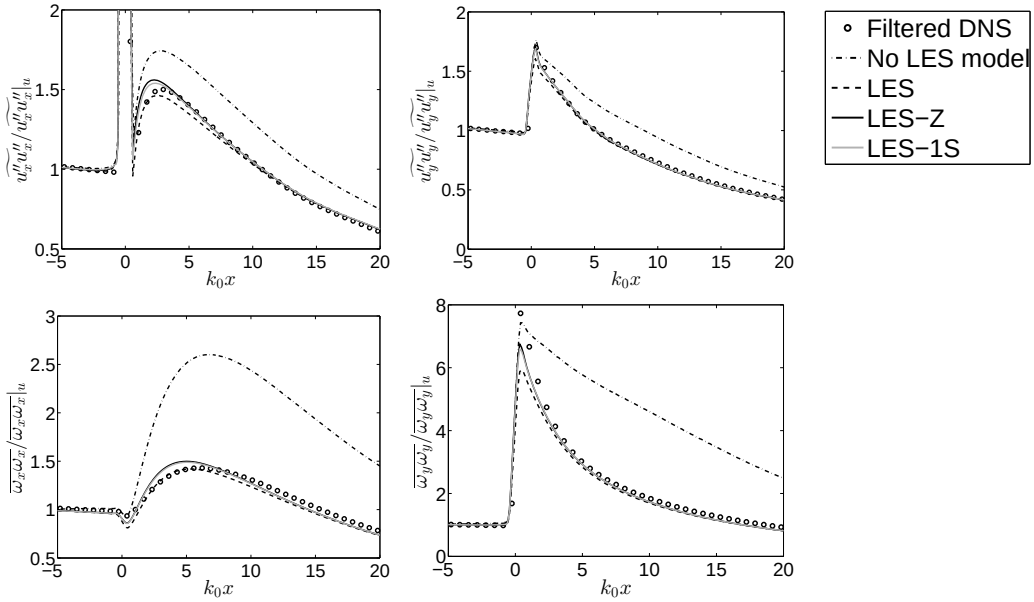

FIGURE 5. Comparison of filtered DNS data of the statistics obtained by LES with different filtering procedures (standard LES, LES-Z and LES-1S) on grid 389×64^2, M = 3. Top row: Reynolds Stress components x (left) and y (right). Bottom row: vorticity components x (left) and y (right).

a two times finer grid (777×128^2) for both M = 1.5 and M = 3 (figure not shown). However, the difference between LES-1S and LES-Z may be more significant for other flow conditions. When in the given problem the shock-capturing scheme dissipation is bigger than SGS dissipation, LES-Z is supposed to obtain the best results. But when

SGS dissipation is bigger than the numerical scheme dissipation, LES-1S is expected to obtain more accurate results than LES-Z.

As we employ implicit LES, the filter width used for obtaining filtered DNS data is not well defined, and therefore filtered DNS data may be considered as a reference solution only contingently. For a more precise comparison of LES filtering modifications, explicit LES will be considered in future.

4. Conclusions

The DNS results obtained by high-order nonlinear filter schemes compare well with the reference solution of Larsson & Lele (2009). In general, the employment of the Yee & Sjögreen filter schemes requires less computational cost than do standard HYBRID schemes. Our LES study confirms results found by previous authors that the dynamic Germano LES model with a standard filtering procedure may lose accuracy due to a strong shock. Two modifications of the LES filtering procedure (LES-Z and LES-1S) designed for improving the accuracy of the standard method have been considered. For this particular shock-turbulence interaction test case, both modifications of the filtering procedure show similar results which are more accurate than the results obtained using the standard LES filtering procedure. However, the turbulent Mach number $\mathrm{M}_t = 0.16$ for the test case considered here is quite low, and the SGS dissipation may be not high enough in comparison with the numerical dissipation of the shock-capturing scheme. Different behavior of considered procedures is expected for high turbulent Mach numbers, with results expected in the near future. In addition, a systematic assessment employing LES-SR and LES-1S will be reported in a forthcoming report. Also, for better estimation of the simulations accuracy the performance of explicitly filtered LES will be considered.

Acknowledgments

The support of the DOE/SciDAC SAP grant DE-AI02-06ER25796 is acknowledged. The authors are grateful to J. Larsson for providing the turbulent inflow and input data. The work has been performed with the first author as a postdoc fellow at the Center for Turbulence Research, Stanford University. Financial support from the NASA Fundamental Aeronautics (Hypersonic) program for the second author is gratefully acknowledged. Work by the fifth author was performed under the auspices of the U.S. Department of Energy by Lawrence Livermore National Laboratory under Contract DE-AC52-07NA27344.

REFERENCES

Adams, N. A. & Stolz, S. 2002 A subgrid-scale deconvolution approach for shock capturing. *J. Comp. Phys.* **178**, 391–426.

Bermejo-Moreno, I., Larsson, J. & Lele, S. K. 2010 LES of canonical shock-turbulence interaction. *Annual Research Briefs,* Center for Turbulence Research, Stanford University, pp. 209–222.

Ducros, F., Ferrand, V., Nicoud, F., Weber, C., Darracq, D., Gacherieu, C. & Poinsot, T. 1999 Large-eddy simulation of the shock/turbulence interaction. *J. Comput. Phys.* **152**, 517–549.

Ducros, F., Laporte, F., Soulères, T., Guinot, V., Moinat, P. & Caruelle, B.

2000 High-order fluxes for conservative skew-symmetric-like schemes in structured meshes: Application to compressible flows. *J. Comp. Phys.* **161**, 114–139.

Erlebacher, G., Hussaini, M. Y., Speziale, C. G. & Zang, T. A. 1992 Toward the large eddy simulation of compressible turbulent flows. *J. Fluid Mech.* **238**, 155.

Germano, M., Piomelli, U., Moin, P. & Cabot, W. 1991 A dynamic subgrid-scale eddy viscosity model. *Phys. Fluids* **3**, 1760–1765.

Grube, N. E. & Martin, M. P. 2009 Assessment of subgrid-scale models and shock-confining filters in large-eddy simulation of highly compressible isotropic turbulence. In *47th AIAA Aerospace Sciences Meeting Including The New Horizons Forum and Aerospace Exposition*.

Hadjadj, A. & Dubos, S. 2009 Large eddy simulation of supersonic boundary layer at $M = 2.4$. In *Proceeding of the IUTAM Symposium on Unsteady Separated Flows and their Control.*

Harten, A. 1989 ENO schemes with subcell resolution. *J. Comp. Phys.* **83**, 148–184.

Larsson, J. & Lele, S. K. 2009 Direct numerical simulation of canonical shock/turbulence interaction. *Phys. Fluids* **21**, 126101.

Lee, S., Lele, S. K. & Moin, P. 1997 Interaction of isotropic turbulence with shock waves: effect of shock strength. *J. Fluid Mech.* **340**, 225–247.

Lilly, D. K. 1992 A proposed modification of the Germano subgrid-scale closure method. *Phys. Fluids* **4**, 633–635.

Lund, T. S. 1997 On the use of discrete fiters for large eddy simulation. *Annual Research Briefs,* Center for Turbulence Research, Stanford University, pp. 83–95.

Olsson, P. 1995 Summation by parts, projections, and stability. I. *Math. Comput.* **64**, 1035–1065.

Olsson, P. & Oliger, J. 1994 *Energy and maximum norm estimates for nonlinear conservation laws.* Technical Report no. 94.01. RIACS.

Ristorcelli, J. R. & Blaisdell, G. A. 1997 Consistent initial conditions for the DNS of compressible turbulence. *Phys. Fluids* **9**, 4–6.

Sagaut, P. & Germano, M. 2005 On the filtering paradigm for LES of flows with discontinuities. *J. Turbul.* **6** (23), 1–9.

Sjögreen, B. & Yee, H. C. 2007 On tenth-order central spatial schemes. In *Proceedings of the Turbulence and Shear Flow Phenomena 5 (TSFP-5).*

Sjögreen, B. & Yee, H. C. 2009 On skew-symmetric splitting and entropy conservation schemes for the euler equations. In *Proc. of the 8th Euro. Conf. on Numerical Mathematics & Advanced Applications (ENUMATH 2009).*

Sjögreen, B., Yee, H. C. & Vinokur, M. 2014 On high order finite-difference metric discretizations satisfying GCL on moving and deforming grids. *J. Comput. Phys.* **265**, 211–220.

Yee, H. & Sjögreen, B. 2002 *Designing adaptive low dissipative high order schemes for long-time integrations.* In: Turbulent Flow Computation (ed. D. Drikakis & B. Geurts). Kluwer Academic.

Yee, H. C. & Sjögreen, B. 2007 Development of low dissipative high order filter schemes for multiscale Navier-Stokes/MHD systems. *J. Comput. Phys.* **225**, 910–934.

Yee, H. C., Vinokur, M. & Djomehri, M. 2000 Entropy splitting and numerical dissipation. *J. Comput. Phys.* **162**, 33–81.